Study of the superconducting order parameter in the two-dimensional negative-U Hubbard model by grand-canonical twist-averaged boundary conditions

Seher Karakuzu,[1] Kazuhiro Seki,[1,2,3] and Sandro Sorella[1]

[1]*International School for Advanced Studies (SISSA), Via Bonomea 265, 34136, Trieste, Italy*

[2]*Computational Materials Science Research Team, RIKEN Center for Computational Science (R-CCS), Hyogo 650-0047, Japan*

[3]*Computational Condensed Matter Physics Laboratory, RIKEN Cluster for Pioneering Research (CPR), Saitama 351-0198, Japan*

(Received 19 June 2018; revised manuscript received 13 August 2018; published 29 August 2018)

By using variational Monte Carlo and auxiliary-field quantum Monte Carlo methods, we perform an accurate finite-size scaling of the s-wave superconducting order parameter and the pairing correlations for the negative-U Hubbard model at zero temperature in the square lattice. We show that the twist-averaged boundary conditions (TABCs) are extremely important to control finite-size effects and to achieve smooth and accurate extrapolations to the thermodynamic limit. We also show that TABCs are much more efficient in the grand-canonical ensemble rather than in the standard canonical ensemble with fixed number of electrons. The superconducting order parameter as a function of the doping is presented for several values of $|U|/t$ and is found to be significantly smaller than the mean-field BCS estimate already for moderate couplings. This reduction is understood by a variational ansatz able to describe the low-energy behavior of the superconducting phase by means of a suitably chosen Jastrow factor including long-range density-density correlations.

DOI: 10.1103/PhysRevB.98.075156

I. INTRODUCTION

In recent years, the numerical simulations have achieved a constantly increasing impact in theoretical and experimental condensed matter physics, because, on one hand it allows reliable solutions of correlated models which cannot be solved analytically [1] and, on the other hand, the quest of accurate benchmark results is now becoming of fundamental importance. From the experimental point of view, the ultracold atom systems have a great flexibility to represent correlated fermionic systems including the Hubbard-like lattice models with either repulsive or attractive interactions. Indeed the emergent collective properties of quantum many-body systems, such as Bose-Einstein condensation (BEC) and superconductivity, can be now probed directly by ultracold atoms trapped in optical lattices [2–5]. These fermionic systems can be represented efficiently by the Hubbard-like lattice models with attractive interaction. Therefore, theoretical and numerical studies on lattice fermions with attractive interactions can provide very useful information and insight for the ultracold atom systems [6].

The negative U two-dimensional (2D) Hubbard model is a very simple model of fermions subject to an attractive interaction on a lattice. It is clearly relevant for studying the standard mechanism of superconductivity within the Bardeen-Cooper-Schrieffer (BCS) theory [7–10]. At finite temperatures, the phase diagram of the model has been investigated by quantum Monte Carlo (QMC) [11–15] as well as by dynamical-mean-field theory calculations [16,17]. Normal (nonsuperconducting) state properties have been studied via finite-temperature Monte Carlo calculations [18] by focusing mainly on the BCS-BEC crossover, and recently [19] the zero temperature quantum critical point between a metal and a superconductor was also satisfactorily described, thanks to large-scale simulations, nowadays possible with modern supercomputers and the excellent algorithmic performances of QMC. At zero temperature, ground-state properties of the model have been also studied by variational Monte Carlo (VMC) calculations as a function of the interaction strength for several electron fillings [20,21]. Recently, an exact QMC calculation of the superconducting gap in an attractive Fermi gas in two dimensions has been reported [6].

As is well known, the main purpose in the numerical simulation is to reach a controlled and accurate thermodynamic limit of a model system with a sequence of calculations with increasing number of electrons. This task may be particularly difficult, especially in the weak-coupling ($|U|/t \ll 8$) regime, because in this limit the location of the Fermi surface plays a crucial role. Indeed, the results obtained with conventional periodic-boundary conditions (PBC) may significantly depend on the particular location of the allowed finite-size momenta, resulting in very difficult, if not impossible, extrapolations to the thermodynamic limit. The drawback of PBC is well known and represents an important limitation of most numerical techniques dealing with fermions. Indeed, an early projector Monte Carlo study has shown strong finite-size effects on superconducting pairing correlations [22]. Obviously, when the Fermi surface is particularly simple such as the 2D-half-filled Hubbard model with its perfectly nested Fermi surface, this problem is less severe but, at weak coupling, even this particular simple case may deserve some attention.

To control the finite size effects discussed above, twist-averaged boundary conditions (TABCs) have been introduced for Monte Carlo simulations on lattice models [23–29] and in continuum systems [30,31]. Within TABCs, physical quantities are estimated by averaging them over several twisted-boundary conditions [32], rather than limiting the calculation to a single twist, such as PBC. In this way, TABCs can substantially reduce finite-size effects [25–28,30], at the expense of performing several independent calculations with

several twists. In QMC, this overhead is not even relevant because, at given computational resources, the statistical errors of the twisted-averaged quantities do not grow with the number N_{TABC} of twists. Thus, this method is particularly appealing within QMC and, quite recently, is becoming widely used for the study of strongly correlated systems. On the other hand, in a recent work [33], by using finite-temperature determinant QMC without TABCs, the convergence of physical quantities to the thermodynamic limit have been examined for the canonical ensemble (CE) and the grand-canonical ensemble (GCE). It has been shown that GCE provides a convergence faster than CE. There are several reasons why this should happen. The simplest one is that only by allowing the fluctuations of the particle number one can ensure that the $U = 0$ Gibbs free energy coincides with the one in the thermodynamic limit [23]. On the other hand, at zero temperature this technique is equivalent to occupy only the electronic states within the given Fermi surface, and this may explain why it is so important for fermionic systems, at least in the weakly correlated regime.

Since the size effects are certainly more pronounced at zero temperature and weak coupling, it is important to explore and benchmark systematically more efficient ways to reduce the finite-size error to assess with some confidence the behavior of the superconducting order parameter—nonzero in 2D only at zero temperature—in the BCS regime.

In this paper, we examine finite-size effects on the s-wave superconducting order parameter and pairing correlations in the 2D negative-U Hubbard model by using VMC and AFQMC methods at zero temperature. The first method can be applied without restrictions to any model, whereas the second method provides numerically exact ground-state properties in models, such as the negative-U Hubbard considered here, not affected by the so-called sign problem. We introduce a combination of TABCs with GCE sampling technique at zero temperature and show that the finite-size effects are more efficiently reduced in GCE than in CE.

The rest of this paper is organized as follows. In Sec. II, we describe the negative-U Hubbard model, VMC and AFQMC methods, and TABCs on a 2D square lattice. In Sec. III, we present numerical results of the s-wave order parameter and the pairing correlation functions for the entire doping range at several values of the interaction strength. In Sec. IV, we draw our conclusions and discuss the implications of the present method for future works.

II. MODEL AND METHOD

A. Negative-U Hubbard model

The Hamiltonian of the negative-U Hubbard model is given as [34]

$$\mathcal{H} = \mathcal{H}_{\mathcal{K}} + \mathcal{H}_{\mathcal{V}} \tag{1}$$

with

$$\mathcal{H}_{\mathcal{K}} = -t \sum_{\langle i,j\rangle,\sigma} (c^{\dagger}_{i\sigma} c_{j\sigma} + \mathrm{H.c.}) - \mu \sum_{i\sigma} n_{i\sigma}, \tag{2}$$

$$\mathcal{H}_{\mathcal{V}} = U \sum_{i} n_{i\uparrow} n_{i\downarrow}, \tag{3}$$

where t is the hopping integral and $\langle i, j\rangle$ indicate nearest-neighbors on a square lattice with $N = L^2$ sites with L being the linear size of the cluster, $c^{\dagger}_{i\sigma}$ ($c_{i\sigma}$) creates (destroys) an electron with spin $\sigma(=\uparrow, \downarrow)$ on the site i, and $n_{i\sigma} = c^{\dagger}_{i\sigma} c_{i\sigma}$. $U < 0$ is the Hubbard interaction term which, in this paper, is considered to be negative and μ is the chemical potential. Hereafter, we set t and the lattice constant, both equal to one.

B. Variational Monte Carlo

To study the negative-U Hubbard Model defined in Eq. (1), we employ the VMC method. As a variational many-body wave function for VMC, we use a Jastrow-Slater wave function of the form

$$|\Psi\rangle = \mathcal{J}|\Psi_{\mathrm{T}}\rangle, \tag{4}$$

where $\mathcal{J}$ is the density-density Jastrow correlator defined by

$$\mathcal{J} = \exp\left(-\frac{1}{2}\sum_{i,j} v_{i,j} n_i n_j\right), \tag{5}$$

with $n_i = \sum_{\sigma} n_{i\sigma}$ and $v_{i,j}$ being the variational parameters which are assumed to depend only on the distance between the sites i and j. It is particularly important to consider in this study a Jastrow factor where the pseudopotential $v_{i,j}$ is nonzero even when the two lattice points are at very large distance d, because in a superconductor the pseudopotential should decay as $\simeq 1/d$ [35] to define a physical wave function with correct charge fluctuations at small momenta. Moreover, when the fluctuations of the number of particles are considered, a fugacity term $\exp(-f \sum_i n_i)$ has to be added to Eq. (5). At half-filling, the fugacity is determined by the condition that Eq. (5) remains unchanged (up to a constant) for the particle-hole symmetry:

$$c_{i\sigma} \rightarrow (-1)^{x_i + y_i} c^{\dagger}_{i-\sigma}, \tag{6}$$

where x_i, y_i are the lattice coordinates of the site i. This implies that $f = \frac{1}{N}\sum_{i,j} v_{i,j}$ after a straightforward calculation.

The antisymmetric part of the wave function, $|\Psi_{\mathrm{T}}\rangle$, is obtained from the ground state of a mean-field (MF) Hamiltonian $\mathcal{H}_{\mathrm{MF}}$ that contains the electron hopping, chemical potential, and singlet s-wave pairing terms:

$$\mathcal{H}_{\mathrm{MF}} = -t \sum_{\langle i,j\rangle,\sigma} (c^{\dagger}_{i\sigma} c_{j\sigma} + \mathrm{H.c.}) - \mu_{\mathrm{BCS}} \sum_{i\sigma} n_{i\sigma} + \Delta_0 \sum_{i} (c^{\dagger}_{i\uparrow} c^{\dagger}_{i\downarrow} + \mathrm{H.c.}), \tag{7}$$

where μ_{BCS}, and Δ_0 are variational parameters. All the variational parameters $v_{i,j}$, μ_{BCS}, and Δ_0 are optimized via stochastic-reconfiguration technique by minimizing the variational expectation value of the energy [36].

To do the Monte Carlo integration, configurations, where electrons have a definite position and spin quantization axis $S^z_i = \pm 1/2$, are sampled through Markov chains and proposed moves are accepted or rejected with the Metropolis algorithm. In particular, it is possible to consider the moves (hoppings) defined by the Hamiltonian of the system of interest. With this limitation, the VMC conserves the total number of particles

and the total projection $S^z_{\rm tot} = \sum_i S^z_i = 0$ of the spin in the chosen quantization axis. Thus, these kind of projections are implicitly assumed in Eq. (4). In this paper, we have also considered moves that change the number of particles (remaining in the $S^z_{\rm tot} = 0$ subspace). With this in mind, one can extend the sampling from CE to GCE by enlarging the Hilbert space, where the former consists of local moves conserving the particle number while the latter includes moves allowing fluctuations of the particle number.

C. Auxiliary-field quantum Monte Carlo

To test the relevance of the correlated ansatz in Eq. (1) for VMC, we also employ the AFQMC method. AFQMC is based on the idea that the imaginary-time propagation of a trial wave function $|\Psi_{\rm T}\rangle$ with a long-enough projection time can project out the exact ground-state wave function $|\Psi_0\rangle$, provided that the trial wave function is not orthogonal to the exact ground-state wave function, i.e., $\langle\Psi_{\rm T}|\Psi_0\rangle \neq 0$ [37]. AFQMC suffers from the negative-sign problem for $U > 0$ if the particle-hole symmetry is broken. However, for the case of the negative-U Hubbard model, there is no sign problem whenever the number of up-spin particles equals the one of down-spin particles [38].

We define a pseudopartition function by [38]

$$\mathcal{Z} = \langle\Psi_{\rm T}|e^{-\beta\mathcal{H}}|\Psi_{\rm T}\rangle = \langle\Psi_{\rm T}|(e^{-\Delta\tau\mathcal{H}})^{2T}|\Psi_{\rm T}\rangle, \tag{8}$$

where β is the projection time and is discretized into $2T$ time slices, i.e., $\Delta\tau = \frac{\beta}{2T}$ in the right-hand side of the above equation. Then the ground-state expectation value of an operator $\mathcal{O}$ can be written as

$$\frac{\langle\Psi_0|\mathcal{O}|\Psi_0\rangle}{\langle\Psi_0|\Psi_0\rangle} = \lim_{T\to\infty} \frac{\langle\Psi_{\rm T}|(e^{-\Delta\tau\mathcal{H}})^T\mathcal{O}(e^{-\Delta\tau\mathcal{H}})^T|\Psi_{\rm T}\rangle}{\mathcal{Z}}. \tag{9}$$

Since the interaction part of the Hamiltonian $\mathcal{H}_V$ consists of a two-body term and does not commute with the kinetic part $\mathcal{H}_K$, the imaginary-time propagator $e^{-\Delta\tau\mathcal{H}}$ requires the following manipulation. First, to factorize the Hamiltonian into the interaction and kinetic parts in the exponential, we use the symmetric Trotter-Suzuki decomposition [39,40]

$$e^{-\Delta\tau\mathcal{H}} = e^{-\frac{\Delta\tau}{2}\mathcal{H}_K} e^{-\Delta\tau\mathcal{H}_V} e^{-\frac{\Delta\tau}{2}\mathcal{H}_K} + O(\Delta\tau^3), \tag{10}$$

where $O(\Delta\tau^3)$ is the systematic error due to the time discretization. Since there are $2T$ number of slices, the errors are accumulated and the resulting systematic error is $O(\Delta\tau^2)$. We set the projection time to be $\beta = 3L$ with a fixed imaginary-time discretization $\Delta\tau = 0.1$. It has been shown that $\Delta\tau = 0.1$ is small enough to accurately determine the ground-state phase diagram of the honeycomb-lattice Hubbard model in the weak-coupling regime [41]. Then, we write the interaction term as a superposition of one-body propagators by means of the well-established Hubbard-Stratonovich transformation [42,43]. Hirsch pointed out that since the occupation numbers are only 0 or 1 for fermions, one can introduce Ising-like discrete fields, $s_i = \pm 1$ [44], such that

$$\begin{aligned}&\prod_i e^{\Delta\tau|U|n_{i,\uparrow}n_{i,\downarrow}} \\ &= \prod_i \frac{1}{2} e^{\frac{\Delta\tau|U|}{2}(n_{i\uparrow}+n_{i\downarrow}-1)} \sum_{s_i=\pm 1} e^{s_i\gamma(n_{i\uparrow}+n_{i\downarrow}-1)},\end{aligned} \tag{11}$$

where $\cosh\gamma = e^{\frac{\Delta\tau|U|}{2}}$. The summation over the auxiliary fields $\{s_i\}$ is performed by the Monte Carlo sampling. For AFQMC, the sampling is done via Markov chains based on local field-flip sequential updates.

When $\Delta_0 = 0$, the trial wave function $|\Psi_{\rm T}\rangle$ is constructed by filling the lowest-lying orbitals for a fixed particle number and therefore the sampling is done in CE. When $\Delta_0 \neq 0$, the sampling is automatically done in GCE, and the desired particle number is obtained by tuning the chemical potential μ. To determine the chemical potential for a desired particle number, we use the Newton-Raphson method, where the average particle number and its derivative with respect to the chemical potential ($\propto$ fluctuation of the particle number) are calculated stochastically by using several AFQMC samplings, a number large enough to guarantee a negligible statistical error (less than .1% on the particle number). The procedure is computationally feasible because the convergence of the chemical potential is achieved within a few Newton-Raphson iterations (typically four iterations are enough). In AFQMC, when using a single twist (and no TABCs), the trial wave function $|\Psi_{\rm T}\rangle$ is the free electron ground state of $\mathcal{H}_\mathcal{K}$, satisfying the closed-shell condition to preserve all the symmetries of the Hamiltonian. On the other hand, for the GCE calculations at finite doping we have used trial wave functions obtained by VMC optimization of the bare chemical potential $\mu_{\rm BCS}$ and a small s-wave pairing [$\sim O(10^{-2}t)$], which allows particle fluctuations within CGE.

D. Twist-averaged boundary conditions

In the case of weakly correlated systems, size effects are most pronounced and calculations of observables with a single boundary condition such as PBC or anti-periodic-boundary condition (APBC) may have serious difficulties in determining the correct thermodynamic limit. To mimic the Brillouin zone of the thermodynamic limit, TABCs have been proposed and indeed it has been shown that TABCs eliminate one-body error very successfully [26,27,30].

On a lattice, by explicitly indicating the coordinates of the site in the creation operators, i.e., $c^\dagger_{i\sigma} \to c^\dagger_{\mathbf{R}_i\sigma}$, where $\mathbf{R}_i = (x_i, y_i)$ denotes the coordinates of the site i in the lattice, twisted-boundary conditions correspond to impose [32]:

$$\begin{aligned}c^\dagger_{\mathbf{R}_i+\mathbf{L_x}\sigma} &= e^{i\theta^\sigma_x} c^\dagger_{\mathbf{R}_i\sigma}, \\ c^\dagger_{\mathbf{R}_i+\mathbf{L_y}\sigma} &= e^{i\theta^\sigma_y} c^\dagger_{\mathbf{R}_i\sigma},\end{aligned} \tag{12}$$

where $\mathbf{L_x} = (L, 0)$ and $\mathbf{L_y} = (0, L)$ are the vectors that define the periodicity of the cluster; θ^σ_x and θ^σ_y are two phases in the interval $(-\pi, \pi)$ determining the twists along x and y directions, respectively. The number of sites is given by $N = L^2$. To preserve time-reversal invariance of the BCS pairs, we imposed that $\theta^\uparrow = -\theta^\downarrow$ in both directions.

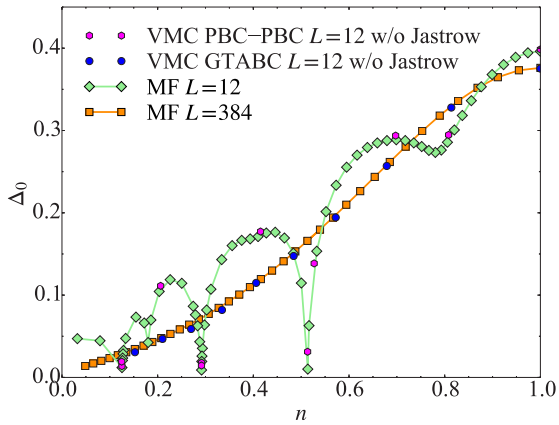

FIG. 1. s-wave variational parameter Δ_0 as a function of n at $U=-2$. Mean-field calculations are performed on $L=12$ and $L=384$ clusters, and VMC calculations are done in GCE without Jastrow correlator on $L=12$ with PBC and TABCs. PBC-PBC indicates PBC in both x and y directions, and w/o stands for without. The error bars in the VMC results are smaller than the symbol sizes.

The expectation value of the operator $\mathcal{O}$ in TABCs is defined by

$$\langle\mathcal{O}\rangle = \frac{1}{N_{\mathrm{TABC}}}\sum_{\theta}\frac{\langle\Psi_\theta|\mathcal{O}_\theta|\Psi_\theta\rangle}{\langle\Psi_\theta|\Psi_\theta\rangle}, \tag{13}$$

where $\theta=(\theta_x^\sigma,\theta_y^\sigma)$, $\mathcal{O}_\theta$ is the operator corresponding to $\mathcal{O}$ under the boundary condition Eq. (12), N_{TABC} is the number of twist angles in the whole Brillouin zone, and $|\Psi_\theta\rangle$ is the wave function $|\Psi\rangle$ for VMC or $|\Psi_0\rangle$ for AFQMC, constructed by imposing the twisted-boundary conditions defined in Eq. (12) to the trial wave function $|\Psi_{\mathrm{T}}\rangle$ as well as to the one-body part of the Hamiltonian. Note, however, that all the wave functions with different θ share the same variational parameters. To perform TABCs, we typically take $N_{\mathrm{TABC}}=1088$ points in the Brillouin zone.

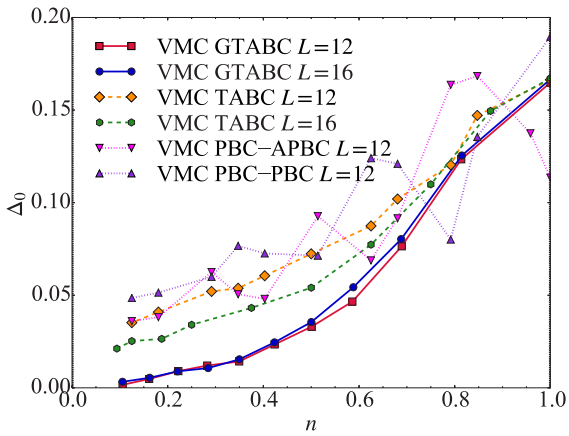

FIG. 2. s-wave variational parameter Δ_0 as a function of n at $U=-2$ calculated by VMC. The system size and boundary conditions used are indicated in the figure. Here, GTABC represents the grand-canonical twist-averaged boundary conditions, TABC the canonical twist-averaged boundary conditions, PBC-APBC stands for PBC in one direction and APBC in the other one, whereas PBC-PBC indicates PBC in both directions. The error bars are smaller than the symbol sizes.

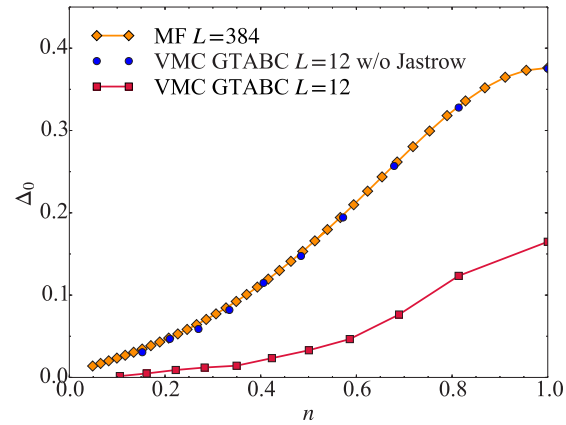

FIG. 3. s-wave variational parameter Δ_0 as a function of n at $U=-2$. The results for mean-field calculations on $L=384$ and VMC on $L=12$ with and without Jastrow correlator in GCE with TABCs are shown. The error bars in the VMC results are smaller than the symbol sizes.

III. RESULTS

A. Size effects in mean-field approximation

Before investigating the finite-size effects in correlated systems, it is instructive to study the finite-size effects within the single-particle theory. For this purpose, we treat the negative-U Hubbard model in Eq. (1) within the self-consistent mean-field approximation by decoupling the interaction term into the s-wave pairing terms.

Figure 1 shows the s-wave superconducting order parameter Δ_0 as a function of electron density n ($n=1$ corresponds to the half-filling) within the mean-field approximation at $U=-2$ for $L=12$ and $L=384$. We have confirmed that the order parameter does not depend on the system size for $L\geq 384$, implying that the results for $L=384$ can be considered very

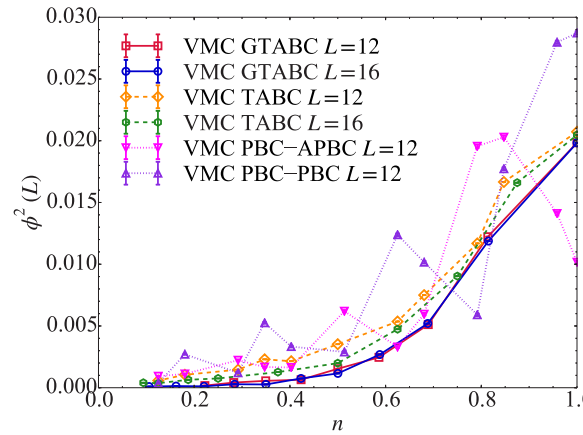

FIG. 4. Pairing correlations ϕ^2 as a function of n at $U=-2$ calculated by VMC. The system size and boundary conditions used are indicated in the figure. The notations are the same as those in Fig. 2.

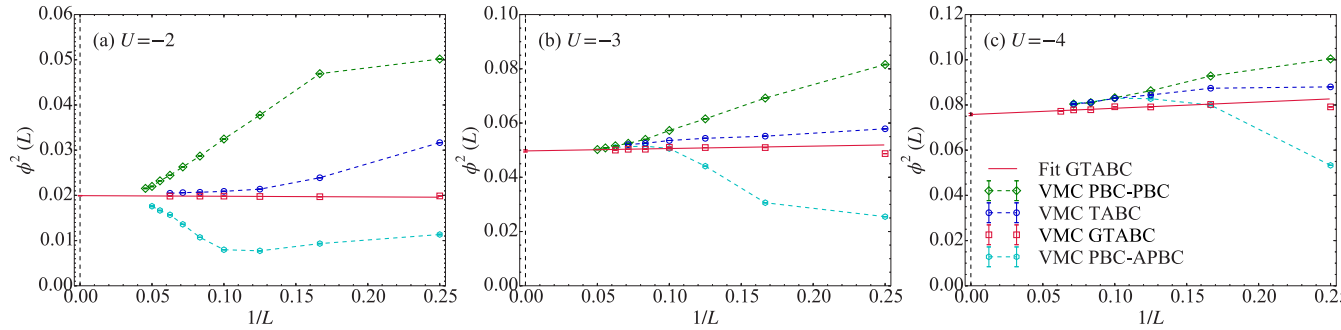

FIG. 5. Finite-size-scaling analyses of the pairing correlation $\phi^2(L)$ for (a) $U=-2$, (b) $U=-3$, and (c) $U=-4$ by VMC at half-filling with different boundary conditions. The solid lines are fits to the GTABC data. The extrapolated values to the thermodynamic limit $\lim_{L\to\infty}\phi^2(L)$ are indicated at $1/L=0$ for each panel and correspond to 0.01994(4) for $U=-2$, 0.0497(4) for $U=-3$, and 0.0758(5) for $U=-4$. The notations are the same as in Fig. 2.

close to the thermodynamic limit. On the other hand, significant size effects, namely the oscillatory dependence on n, are observed for $L=12$.

To test the accuracy of our VMC calculation, we have reproduced the above results by setting the Jastrow correlator $\mathcal{J}$ in Eq. (4) to be unity, i.e., $v_{i,j}=0$. The VMC calculations are performed for $L=12$, using a single twist or 32×32 twist angles in the whole Brillouin zone. Notice that the latter case corresponds, within a mean-field approach, to a single calculation with $L=384$ and PBC. The results obtained by VMC in GCE without Jastrow part are indeed in perfect agreement with those obtained independently by the mean-field calculation.

B. *s*-wave variational parameter

The mean-field results do not take into account the correlations between the electrons. The accuracy for treating the electron correlations can be improved by including the Jastrow factor in Eq. (4). Figure 2 shows the superconducting variational parameter Δ_0 as a function of electron density n within VMC for $L=12$ and $L=16$ with different boundary conditions and different ensembles. For a fixed system size of $L=12$, the results with a single boundary condition show oscillatory dependencies on n, similarly to the ones obtained within the mean-field approximation for $L=12$. With TABCs in both ensembles, the oscillatory dependencies are significantly reduced. By further increasing the system size to $L=16$, a sizable decrease of Δ_0 is observed in CE especially for the low-density regime, while the change in GCE is almost negligible, indicating that the GCE shows much smaller size effects.

Having confirmed the significant reduction of the finite-size effects, we show in Fig. 3 how the Jastrow correlator affects the magnitude of the optimal variational parameter. By using the same system size of $L=12$ with the same number of twist angles, the Jastrow correlator reduces the magnitude of the *s*-wave variational parameter by more than a factor two for $n=1$. Note that this systematic comparison of the variational wave function with and without the Jastrow correlator for the entire doping range has been made possible only with GTABCs, because the results with a single boundary condition exhibit oscillatory behaviors both in the mean-field approximation and VMC.

C. Pairing correlation function

The finite order or variational parameters observed in the mean-field approximation or the VMC for finite-size systems are due to the wave function ansatz that explicitly breaks the U(1) symmetry. To compare the VMC results with the ones of the numerically exact AFQMC, it is necessary to study the off-diagonal long-range order by computing superconducting correlation functions. To this purpose, we consider the *s*-wave

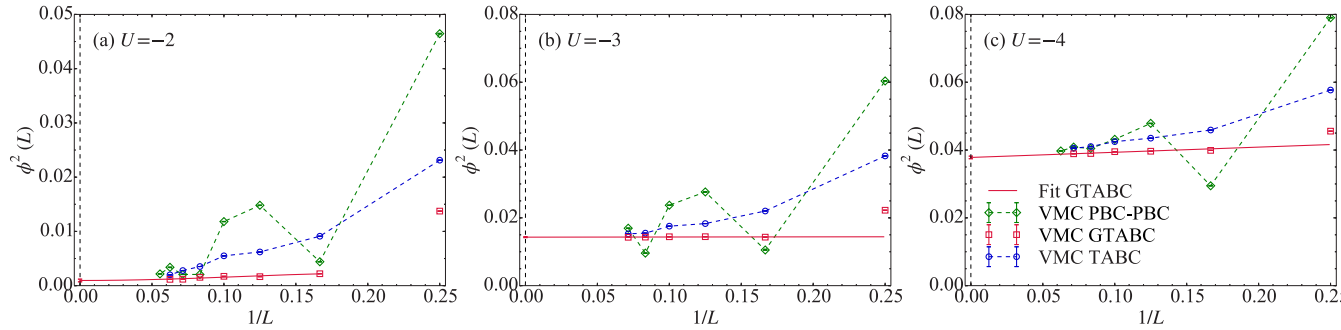

FIG. 6. Finite-size-scaling analyses of the pairing correlation $\phi^2(L)$ for (a) $U=-2$, (b) $U=-3$, and (c) $U=-4$ by VMC at quarter-filling with different boundary conditions. The solid lines are fits to the GTABC data. The extrapolated values to the thermodynamic limit $\lim_{L\to\infty}\phi^2(L)$ are indicated at $1/L=0$ for each panel and correspond to 0.00095(25) for $U=-2$, 0.0143(1) for $U=-3$, and 0.0378(4) for $U=-4$. The notations are the same as those in Fig. 2.

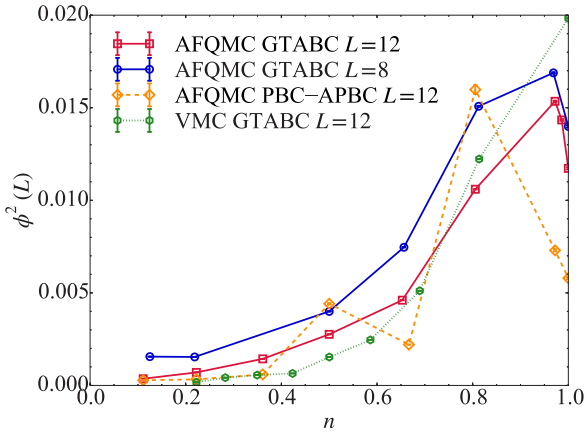

FIG. 7. Pairing correlation ϕ^2 as a function of n at $U = -2$ by AFQMC and VMC. The system size and boundary conditions are indicated in the figure. The notations are the same as in Fig. 2.

pairing correlation function

$$\phi^2(L) = \frac{1}{2N}\sum_i \langle \Delta_i^\dagger \Delta_{i+j} + \text{H.c.}\rangle, \tag{14}$$

where $\Delta_i^\dagger = c_{i\uparrow}^\dagger c_{i\downarrow}^\dagger$ and i and $i + j$ are sites at the maximum distance allowed by the boundary conditions of the cluster.

Figure 4 shows the calculated pairing correlation functions with VMC for various boundary conditions. As in the case of the variational parameter discussed in the previous section, strong finite-size effects are observed for $L = 12$ with a single boundary condition. By increasing the system size to $L = 16$, TABCs with CE reduce the oscillatory dependence as a function of n, but only with GCE the size effects become almost negligible within the available cluster sizes.

Careful finite-size-scaling analyses for the pairing correlation functions are done for $U = -2, -3$, and -4 at half-filling and at quarter-filling in Figs. 5 and 6, respectively. We observe that, even at half-filling, it is almost impossible to extrapolate the pairing correlations with a single twist since this approximation changes behavior as the system size increases, especially when the value of the $|U|$ is small. Instead, it is clearly evident that the TABCs with GCE represents the best method to deal with finite size effects, also much better than TABCs within CE. In particular, at quarter-filling, severe system-size dependencies of the correlation functions are observed, implying that the finite-size scaling with a single twist is almost impossible.

Figure 7 shows the pairing correlations obtained with AFQMC for $L = 8$ and $L = 12$ as well as VMC in GCE on $L = 12$. As in the case of VMC, the PBC results show significant size effects that are reduced significantly by GTABCs also for AFQMC. Close to half-filling, within AFQMC, the value of ϕ^2 becomes larger than the corresponding one at half-filling, a behavior qualitatively different from the one observed within VMC. This effect has been reported in the early QMC study of the negative-U Hubbard model [11], and can be attributed to the spin-flop transition in the strong-coupling limit, where the model at small doping can be mapped to the Heisenberg model in presence of a small magnetic field (see also Sec. III D). In this case, as soon a nonzero magnetic field is present the order parameter "flops" in the xy plane.

Despite GTABCs, visible size effects remain in Fig. 7 for the AFQMC case, and we have therefore focused on a few filling values, that we have systematically studied as a function of the system size. We show the finite-size scaling of the pairing correlations at half-filling and at quarter-filling calculated by AFQMC in Figs. 8 and 9, respectively. As expected from the previous VMC study, also in the case of AFQMC calculations, the TABCs with GCE allow a finite size scaling much better than the one with a single boundary condition. At half-filling, the values of ϕ^2 extrapolated to the thermodynamic limit are therefore computed with high accuracy, as shown in Fig. 8.

At quarter-filling, the situation is even worse for the single twist approach, and severe system-size dependencies of the correlation functions prevent a systematic extrapolation to the thermodynamic limit. Fortunately, this remains possible within TABC approach and controlled extrapolations can be done also for AFQMC calculations. The thermodynamic values of superconducting correlations are therefore computed with high accuracy, as shown in Fig. 9.

D. Attractive-repulsive mapping and order parameters

The negative-U Hubbard model can be mapped to the positive-U Hubbard model with the particle-hole

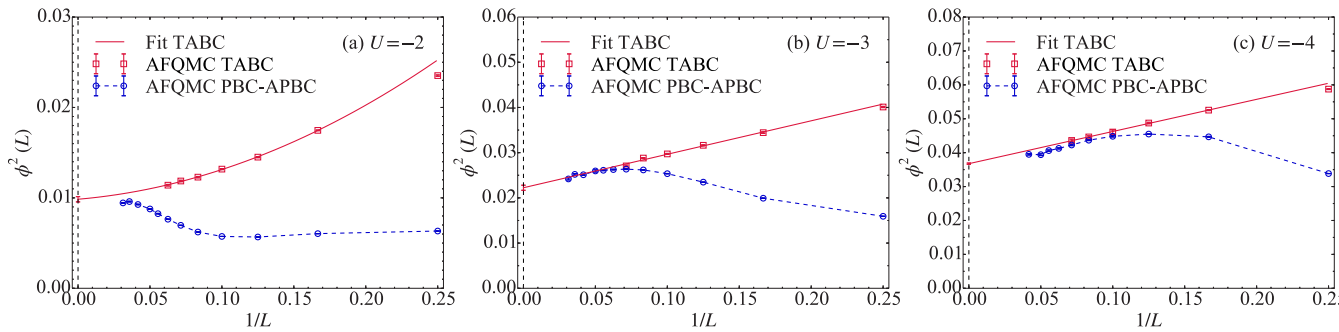

FIG. 8. Finite-size-scaling analyses of the pairing correlation $\phi^2(L)$ for (a) $U = -2$, (b) $U = -3$, and (c) $U = -4$ by AFQMC at half-filling with different boundary conditions. The solid lines are the fit to the TABC data. The TABC extrapolated values to the thermodynamic limit $\lim_{L\to\infty}\phi^2(L)$ are indicated at $1/L = 0$ for each panel and correspond to 0.0098(3) for $U = -2$, 0.0222(6) for $U = -3$, and 0.0368(2) for $U = -4$. The notations are the same as those in Fig. 2.

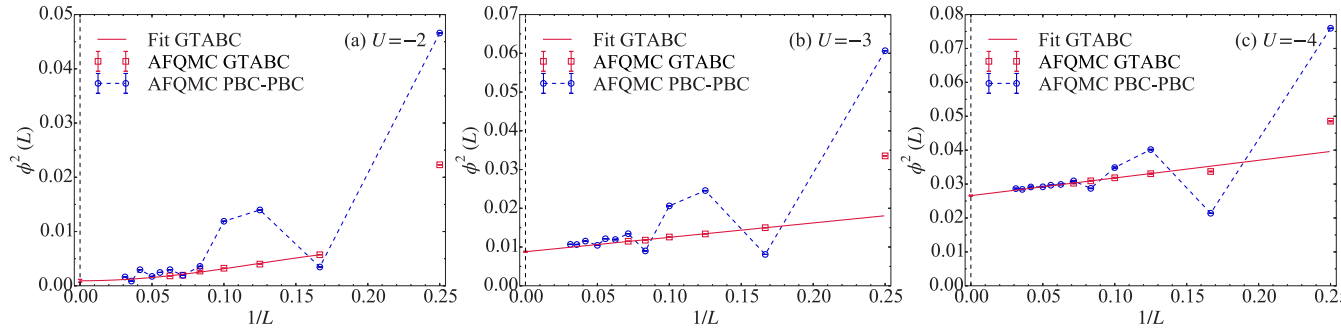

FIG. 9. Finite-size-scaling analyses of the pairing correlation $\phi^2(L)$ for (a) $U=-2$, (b) $U=-3$, and (c) $U=-4$ by AFQMC at quarter-filling with different boundary conditions. The solid lines are the fit to the GTABC data. The GTABC extrapolated values to the thermodynamic limit $\lim_{L\to\infty}\phi^2(L)$ are indicated at $1/L=0$ for each panel and correspond to 0.0009(3) for $U=-2$, 0.0088(1) for $U=-3$, and 0.0266(2) for $U=-4$. The notations are the same as those in Fig. 2.

transformation [45]:

$$\tilde{c}_{i\uparrow} := c_{i\uparrow}, \tag{15}$$

$$\tilde{c}_{i\downarrow} := (-1)^{x_i+y_i} c^{\dagger}_{i\downarrow}. \tag{16}$$

This mapping allows us to compare the results of the pairing correlation function $\phi^2(L)$ with those of the transverse spin-spin correlation function in the positive-U Hubbard model. Indeed, in terms of the newly defined operators $\tilde{c}_{i\sigma}$, $\tilde{c}^{\dagger}_{i\sigma}$, and $\tilde{n}_{i\sigma}=\tilde{c}^{\dagger}_{i\sigma}\tilde{c}_{i\sigma}$, the Hamiltonian changes, up to a constant, to

$$H = -t\sum_{\langle i,j\rangle,\sigma}(\tilde{c}^{\dagger}_{i\sigma}\tilde{c}_{j\sigma}+\text{H.c.}) + |U|\sum_i \tilde{n}_{i\uparrow}\tilde{n}_{i\downarrow} - \sum_i[(\mu-U)\tilde{n}_{i\uparrow}-\mu\tilde{n}_{i\downarrow}], \tag{17}$$

TABLE I. Comparison of the s-wave superconducting (antiferromagnetic) order parameter M_0 defined in Eq. (19) for the negative (positive)-U Hubbard model at half-filling ($n=1$). For the VMC case, we have not included the factor $\sqrt{\frac{3}{2}}$, see discussion in the conclusions. The number in each parenthesis in this paper indicates the uncertainty due to the extrapolation to the thermodynamic limit. The AFQMC simulations in Ref. [46] are performed with the modified-boundary conditions, while in Refs. [1] and [28] with the TABCs method. DMET stands for density-matrix-embedding theory, CDMET for cluster DMET, DCA-DMET for dynamical-cluster-approximation DMET, and MF for the standard BCS mean-field theory.

	$n=1$		
$\lvert U\rvert/t$	2	3	4
MF	0.1881	0.2830	0.3453
VMC (this paper)	0.1412(1)	0.2230(6)	0.2752(6)
AFQMC (this paper)	0.122(1)	0.183(2)	0.2347(4)
AFQMC [46]	0.120(5)	–	–
AFQMC [28]	0.119(4)	–	0.236(1)
DMET [1]	0.133(5)	–	0.252(9)
CDMET [47]	0.115(2)	–	0.226(3)
DCA-DMET [47]	0.120(2)	–	0.227(2)

whereas $\phi^2(L)$ can be written as the transverse spin-spin correlation function:

$$M^2_{xy}(L) = \frac{1}{2N}\sum_i (-1)^{x_j+y_j}\langle S^+_i S^-_{i+j}+\text{H.c.}\rangle = \frac{1}{N}\sum_i (-1)^{x_j+y_j}\langle S^x_i S^x_{i+j}+S^y_i S^y_{i+j}\rangle, \tag{18}$$

where $S^+_i=\tilde{c}^{\dagger}_{i\uparrow}\tilde{c}_{i\downarrow}$, $S^-_i=(S^+_i)^{\dagger}$, $S^x_i=(S^+_i+S^-_i)/2$, and $S^y_i=(S^+_i-S^-_i)/2\text{i}$. Similarly, the charge-charge correlations in the negative-U Hubbard model can be mapped to the longitudinal spin-spin correlations in the positive-U Hubbard model. In the present study, however, the charge-charge correlations are not considered as they will not dominate over the pairing correlations for large distances away from the half-filling.

Since the negative-U Hubbard model with $\mu=U/2$ (the half-filled case) corresponds to the positive-U Hubbard model with zero magnetic field, the SU(2) symmetric staggered magnetization M_0 in the thermodynamic limit can be estimated from $M_{xy}(L)$ through the relation

$$M_0 = \sqrt{\frac{3}{2}\lim_{L\to\infty} M^2_{xy}(L)}, \tag{19}$$

where the factor 3/2 within the square root is included to take into account the contribution from the longitudinal spin-spin correlation which is not present in $M^2_{xy}(L)$. The estimated values of M_0 are reported in Table I. For $|U|=2$ and 4, these values are in agreement with a recent study [28] and, for $|U|=2$, also with a previous work [46] by one of us.

TABLE II. Comparison of the s-wave superconducting order parameter Φ_s defined in Eq. (20) for the negative-U Hubbard model at quarter-filling ($n=0.5$). The number in each parenthesis in this paper indicates the uncertainty due to the extrapolation to the thermodynamic limit.

	$n=0.5$		
$\lvert U\rvert/t$	2	3	4
VMC (this paper)	0.031(4)	0.1196(6)	0.194(1)
AFQMC (this paper)	0.030(4)	0.094(1)	0.163(1)

TABLE III. Comparison of the ground-state energies for the negative (positive)-U Hubbard model at half-filling ($n = 1$). The number in each parenthesis in this paper indicates the uncertainty due to the extrapolation to the thermodynamic limit.

$n = 1$			
$\|U\|/t$	2	3	4
VMC (this paper)	−2.16848(1)	−2.49007(1)	−2.84769(5)
AFQMC (this paper)	−2.1755(3)	−2.5014(3)	−2.86016(9)
AFQMC [46]	−2.175469(92)	−2.501412(52)	–
AFQMC [28]	−2.1760(2)	–	−2.8603(2)
AFQMC [1]	−2.1763(2)	–	−2.8603(2)
DMET [1]	−2.1764(3)	–	−2.8604(3)
CDMET [47]	−2.1756(3)	–	−2.8600(1)
DCA-DMET [47]	−2.1755(2)	–	−2.8600(2)

At quarter-filling, the CDW order disappears and we are left to study only the s-wave order parameter defined as

$$\Phi_s = \sqrt{\lim_{L\to\infty} \phi^2(L)}. \tag{20}$$

The estimated values of Φ_s from the extrapolated values of $\phi^2(L)$ are reported in Table II.

To test the accuracy of the variational wave function in the thermodynamic limit, we have also compared the VMC estimates of the ground-state energies with the AFQMC ones in Tables III and IV at half-filling and at quarter-filling, respectively. The energies obtained via AFQMC in the present study are in agreement with the exact energies of previous works. It is worth mentioning that VMC energies are providing quite good upper bounds to the exact energies, especially in the weak-coupling regime.

IV. CONCLUSIONS AND DISCUSSIONS

To conclude, finite-size effects on the s-wave order parameter and pairing correlation functions have been studied in detail for the negative-U Hubbard model with VMC and AFQMC methods. For both methods, GTABCs reduce systematically the finite size effects and provide smooth extrapolation to the thermodynamic limit. This has enabled us to obtain well-converged results on energy and order parameter for several values of U/t and doping, and to study very efficiently the physical properties in the thermodynamic limits of our Jastrow correlated wave function as a function of doping. Indeed, we have shown that our variational wave function is not only qualitatively correct, but also quantitatively, as the magnitude of the s-wave variational parameter is significantly reduced in the entire doping range, already at $U = -2$, in agreement with the exact AFQMC result. The success of VMC in this particular case, where the exact solution is available, is important because VMC can be easily extended [26] to any model, even the ones affected by the sign problem within AFQMC.

We have also presented the comparison of the pairing correlation functions obtained by VMC and by the numerically exact AFQMC. In this case, VMC is in good agreement with AFQMC for finite doping. At half-filling, there exists a pseudo-SU(2) symmetry defined by the SU(2) rotations in spin space applied to the Hamiltonian after the particle-hole transformation in Eq. (15), that remains therefore invariant and commuting with the pseudospin operators [the spin operators after the particle-hole transformation of Eq. (15)]. This symmetry is clearly accidental, as is no longer satisfied by the inclusion of a tiny next-nearest-neighbor hopping t' [19]. Since our variational wave function breaks this accidental pseudo-SU(2) symmetry, the agreement between the VMC and the necessarily symmetrical (as the exact ground state in any finite lattice is a singlet after particle-hole transformation [48]) AFQMC in this case is not very good just because, in the VMC, the order is only in one of the possible directions of a three-component order parameter. For this reason, when comparing VMC and AFQMC in Table I, we have not included in the VMC entries the factor $\sqrt{3/2}$ implied by the definition of M_0 in Eq. (19), as we have verified that, within VMC, the order is in the xy plane, because the CDW order, corresponding, in the positive-U language, to the z component of the antiferromagnetic order parameter, is always negligible. This consideration explains also why the spin-flop transition observed in AFQMC—M_{xy} jumps to a larger value as soon as we depart from half-filling—is not present in VMC, because, as shown in Fig. 7, M_{xy} appears a smooth and monotonically decreasing function of the doping.

Apart from symmetry considerations that can be restored by standard symmetry projection techniques [49,50], our wave function can be also improved, for example, by taking into account the backflow correlations [51], as it was done in the positive-U Hubbard model [52,53].

The method for reducing finite-size effects, developed in this paper, is applicable for any correlated lattice model. The calculation in GCE will be particularly useful for investigating the doping dependence of the d-wave superconductivity in the positive-U Hubbard model with parameters

TABLE IV. Comparison of the ground-state energies for the negative-U Hubbard model at quarter-filling ($n = 0.5$). The number in each parenthesis in this paper indicates the uncertainty due to the extrapolation to the thermodynamic limit.

$n = 0.5$			
$\|U\|/t$	2	3	4
VMC (this paper)	−1.4615(2)	−1.55820(6)	−1.68016(4)
AFQMC (this paper)	−1.4652(5)	−1.5669(5)	−1.6920(2)

relevant for cuprates. Furthermore, the reduction of the order parameter in the entire doping range due to the Jastrow factor suggests that the electron-correlation is not negligible even for weakly attracting fermions in the low-electron-density regime. This implies that the method will be also promising for studying the ground-state properties of dilute electron systems. Such systems may include $TiSe_2$ in the series of transition metal dichalcogenides [54–57], where its electronic state is in vicinity of the semimetal-semiconductor transition and considered to be a candidate of excitonic insulators, in which coherent electron-hole pairs are formed and condensate spontaneously [58,59].

ACKNOWLEDGMENTS

We acknowledge Federico Becca for useful discussions. Computational resources were provided mostly by CINECA and partly by HOKUSAI GreatWave facility at RIKEN under the Project No. G18007. K. S. acknowledges support from the JSPS Overseas Research Fellowships.

[1] J. P. F. LeBlanc, A. E. Antipov, F. Becca, I. W. Bulik, Garnet Kin-Lic Chan, C.-M. Chung, Y. Deng, M. Ferrero, T. M. Henderson, C. A. Jiménez-Hoyos, E. Kozik, X.-W. Liu, A. J. Millis, N. V. Prokof'ev, M. Qin, G. E. Scuseria, H. Shi, B. V. Svistunov, L. F. Tocchio, I. S. Tupitsyn, S. R. White, S. Zhang, B.-X. Zheng, Z. Zhu, and E. Gull (Simons Collaboration on the Many-Electron Problem), Phys. Rev. X **5**, 041041 (2015).

[2] S. Inouye, M. R. Andrews, J. Stenger, H.-J. Miesner, D. M. Stamper-Kurn, and W. Ketterle, Nature **392**, 151 (1998).

[3] P. Courteille, R. S. Freeland, D. J. Heinzen, F. A. van Abeelen, and B. J. Verhaar, Phys. Rev. Lett. **81**, 69 (1998).

[4] M. Greiner, C. A. Regal, and D. S. Jin, Nature **426**, 537 (2003).

[5] I. Bloch, J. Dalibard, and W. Zwerger, Rev. Mod. Phys. **80**, 885 (2008).

[6] E. Vitali, H. Shi, M. Qin, and S. Zhang, Phys. Rev. A **96**, 061601 (2017).

[7] J. Bardeen, L. N. Cooper, and J. R. Schrieffer, Phys. Rev. **108**, 1175 (1957).

[8] A. J. Leggett, in *Modern Trends in the Theory of Condensed Matter*, edited by A. Pekalski and J. A. Przystawa (Springer, Berlin, 1980), pp. 13–27.

[9] R. Micnas, J. Ranninger, and S. Robaszkiewicz, Rev. Mod. Phys. **62**, 113 (1990).

[10] P. Nozières and S. Schmitt-Rink, J. Low Temp. Phys. **59**, 195 (1985).

[11] R. T. Scalettar, E. Y. Loh, J. E. Gubernatis, A. Moreo, S. R. White, D. J. Scalapino, R. L. Sugar, and E. Dagotto, Phys. Rev. Lett. **62**, 1407 (1989).

[12] A. Moreo and D. J. Scalapino, Phys. Rev. Lett. **66**, 946 (1991).

[13] J. M. Singer, M. H. Pedersen, T. Schneider, H. Beck, and H.-G. Matuttis, Phys. Rev. B **54**, 1286 (1996).

[14] J. Singer, T. Schneider, and M. Pedersen, Eur. Phys. B.: Condens. Matter Complex Sys. **2**, 17 (1998).

[15] A. Moreo, D. J. Scalapino, and S. R. White, Phys. Rev. B **45**, 7544 (1992).

[16] A. Toschi, M. Capone, and C. Castellani, Phys. Rev. B **72**, 235118 (2005).

[17] A. Toschi, P. Barone, M. Capone, and C. Castellani, New J. Phys. **7**, 7 (2005).

[18] M. Randeria, N. Trivedi, A. Moreo, and R. T. Scalettar, Phys. Rev. Lett. **69**, 2001 (1992).

[19] Y. Otsuka, K. Seki, S. Sorella, and S. Yunoki, Phys. Rev. B **98**, 035126 (2018).

[20] S. Tamura and H. Yokoyama, J. Phys. Soc. Jpn. **81**, 064718 (2012).

[21] H. Yokoyama, Prog. Theor. Phys. **108**, 59 (2002).

[22] D. Bormann, T. Schneider, and M. Frick, Europhys. Lett. **14**, 101 (1991).

[23] C. Gros, Z. Phys. B: Condens. Matter **86**, 359 (1992).

[24] C. Gros, Phys. Rev. B **53**, 6865 (1996).

[25] T. Koretsune, Y. Motome, and A. Furusaki, J. Phys. Soc. Jpn. **76**, 074719 (2007).

[26] S. Karakuzu, L. F. Tocchio, S. Sorella, and F. Becca, Phys. Rev. B **96**, 205145 (2017).

[27] M. Dagrada, S. Karakuzu, V. L. Vildosola, M. Casula, and S. Sorella, Phys. Rev. B **94**, 245108 (2016).

[28] M. Qin, H. Shi, and S. Zhang, Phys. Rev. B **94**, 085103 (2016).

[29] E. Vitali, H. Shi, M. Qin, and S. Zhang, Phys. Rev. B **94**, 085140 (2016).

[30] C. Lin, F. H. Zong, and D. M. Ceperley, Phys. Rev. E **64**, 016702 (2001).

[31] S. Chiesa, D. M. Ceperley, R. M. Martin, and M. Holzmann, Phys. Rev. Lett. **97**, 076404 (2006).

[32] D. Poilblanc, Phys. Rev. B **44**, 9562 (1991).

[33] Z. Wang, F. F. Assaad, and F. Parisen Toldin, Phys. Rev. E **96**, 042131 (2017).

[34] J. Hubbard, Proc. R. Soc. London **276**, 238 (1963).

[35] M. Capello, F. Becca, M. Fabrizio, S. Sorella, and E. Tosatti, Phys. Rev. Lett. **94**, 026406 (2005).

[36] S. Sorella, Phys. Rev. B **71**, 241103 (2005).

[37] S. Sorella, S. Baroni, R. Car, and M. Parrinello, Europhys. Lett. **8**, 663 (1989).

[38] F. Becca and S. Sorella, *Quantum Monte Carlo Approaches for Correlated Systems* (Cambridge University Press, Cambridge, 2017).

[39] H. F. Trotter, Proc. Am. Math. Soc. **10**, 545 (1959).

[40] M. Suzuki, Comm. Math. Phys. **51**, 183 (1976).

[41] S. Sorella, Y. Otsuka, and S. Yunoki, Sci. Rep. **2**, 992 (2012).

[42] J. Hubbard, Phys. Rev. Lett. **3**, 77 (1959).

[43] R. L. Stratonovich, Dokl. Akad. Nauk. SSSR **115**, 1097 (1957).

[44] J. E. Hirsch, Phys. Rev. B **31**, 4403 (1985).

[45] H. Shiba, Prog. Theor. Phys. **48**, 2171 (1972).

[46] S. Sorella, Phys. Rev. B **91**, 241116 (2015).

[47] B.-X. Zheng, J. S. Kretchmer, H. Shi, S. Zhang, and Garnet Kin-Lic Chan, Phys. Rev. B **95**, 045103 (2017).

[48] E. H. Lieb, Phys. Rev. Lett. **62**, 1201 (1989).

[49] D. Tahara and M. Imada, J. Phys. Soc. Jpn. **77**, 114701 (2008).

[50] R. Rodríguez-Guzmán, K. W. Schmid, C. A. Jiménez-Hoyos, and G. E. Scuseria, Phys. Rev. B **85**, 245130 (2012).

[51] M. Holzmann, D. M. Ceperley, C. Pierleoni, and K. Esler, Phys. Rev. E **68**, 046707 (2003).
[52] L. F. Tocchio, F. Becca, A. Parola, and S. Sorella, Phys. Rev. B **78**, 041101 (2008).
[53] L. F. Tocchio, F. Becca, and C. Gros, Phys. Rev. B **83**, 195138 (2011).
[54] C. Monney, E. F. Schwier, M. G. Garnier, N. Mariotti, C. Didiot, H. Cercellier, J. Marcus, H. Berger, A. N. Titov, H. Beck, and P. Aebi, New J. Phys. **12**, 125019 (2010).
[55] K. Rossnagel, J. Phys.: Condens. Matter **23**, 213001 (2011).
[56] H. Watanabe, K. Seki, and S. Yunoki, Phys. Rev. B **91**, 205135 (2015).
[57] T. Kaneko, Y. Ohta, and S. Yunoki, Phys. Rev. B **97**, 155131 (2018).
[58] D. Jérome, T. M. Rice, and W. Kohn, Phys. Rev. **158**, 462 (1967).
[59] B. I. Halperin and T. M. Rice, Rev. Mod. Phys. **40**, 755 (1968).